Structural Monitoring and Maintenance, *Vol. 1, No. 3 (2014) 339-356*
DOI: http://dx.doi.org/10.12989/smm.2014.1.3.339

Impedance-based damage monitoring of steel column connection: numerical simulation

Duc-Duy Ho[1a], Thanh-Mong Ngo[1b] and Jeong-Tae Kim[*2]

[1]*Faculty of Civil Engineering, Ho Chi Minh City University of Technology, Ho Chi Minh City, Vietnam*
[2]*Department of Ocean Engineering, Pukyong National University, Busan 608-737, Korea*

(Received May 20, 2014, Revised August 16, 2014, Accepted September 4, 2014)

Abstract. This study has been motivated to evaluate the practicality of numerical simulation of impedance monitoring for damage detection in steel column connection. In order to achieve the objective, the following approaches are implemented. Firstly, the theory of electro-mechanical (E/M) impedance responses and impedance-based damage monitoring method are outlined. Secondly, the feasibility of numerical simulation of impedance monitoring is verified for several pre-published experimental examples on steel beams, cracked aluminum beams, and aluminum round plates. Undamaged and damaged steel and aluminum beams are simulated to compare to experimental impedance responses. An aluminum round plate with PZT patch in center is simulated to investigate sensitive range of impedance responses. Finally, numerical simulation of the impedance-based damage monitoring is performed for a steel column connection in which connection bolts are damaged. From the numerical simulation test, the applicability of the impedance-based monitoring to the target steel column connection can be evaluated.

Keywords: electro-mechanical impedance; PZT sensor; damage monitoring; numerical simulation; steel column connection; bolted connection

1. Introduction

During service life of civil structures, the occurrence of damages is inevitable. If the damages are not detected timely, they will cause catastrophic incidents for the safety of not only self-structures but also the humans. Therefore, structural health monitoring (SHM) becomes an important technology and plays a significant role in the safety and service life of civil structures. One of the promising ways to guarantee the structural safety and integrity is to enact SHM in a regular periodic manner and to detect critical damage in its early stage (Doebling *et al*. 1998, Farrar 2001, Kim *et al*. 2014, Li *et al*. 2014). As the concern is limited to the SHM in civil infrastructures, there have been many research attempts on structural response analysis, development of new sensing mechanism, adaptation of SHM method suitable to the structure, and field evaluation and application. Along with the research track, this study focuses on impedance-based SHM technique.

*Corresponding author, Professor, E-mail: idis@pknu.ac.kr
[a] Lecturer
[b] Graduate Student

http://www.techno-press.org/?journal=smm&subpage=7 ISSN: 2288-6605 (Print), 2288-6613 (Online)

Recently, impedance-based damage monitoring technologies have been widely used in SHM applications (Liang *et al*. 1994, Sun *et al*. 1995, Park *et al*. 2003, Giurgiutiu and Zagrai 2005, Kim *et al*. 2010, Ho 2012). This non-destructive testing (NDT) technique bases on the change in structural electro-mechanical (E/M) characteristics which are measured by piezoelectric sensor such as PZT (Lead Zirconate Titanate) patch surface-bonded to the host structure. The PZT patch's electrical impedance responses are directly related to the host structure's mechanical impedance responses. In comparison to host structure, the dimensions and weight of PZT patch are very thin; therefore, they do not influence the structural dynamic characteristics of host structure.

The basic concept of the impedance-based damage monitoring methods is to monitor the changes in structural mechanical impedance caused by the presence of damage. The impedance-based SHM methods are useful to detect damage in critical local members. Those methods are sensitive to small incipient damage. The use of impedance signatures for damage detection was first proposed by Liang *et al*. (1994). Since then, many researchers have improved and applied the method to various damage detection problems. To monitor the occurrence of damage, Sun *et al*. (1995) proposed a simple statistical algorithm based on the root mean square deviation (RMSD) of impedance signatures. Raju *et al*. (1998) suggested another method based on the correlation coefficient (CC) of impedance signatures. Zagrai and Giurgiutiu (2001) investigated several statistical methods including RMSD, mean absolute percentage deviation, covariance change, and correlation coefficient deviation. The impedance-based methods have been successfully applied to truss structures (Sun *et al*. 1995), steel bridge sections (Ayres *et al*. 1998), composite structures (Chaudhry *et al*. 1996, Pohl *et al*. 2001), concrete structures (Soh *et al*. 2000, Park *et al*. 2006), steel structures (Park *et al*. 2005), thin plates and aerospace structures (Giurgiutiu and Zagrai 2005), prestress-loss in PSC girders (Kim *et al*. 2010), bolted connection in full-scale steel bridge (Min *et al*. 2010), and full-scale cable-stayed bridge (Ho 2012).

In this paper, the practicality of numerical simulation of impedance monitoring for damage detection in steel column connection is evaluated. In order to achieve the objective, the following approaches are implemented. Firstly, the theory of impedance-based damage monitoring is outlined. Secondly, the feasibility of numerical simulation of impedance monitoring is verified for several pre-published experimental examples on steel beams, aluminum beams, and aluminum round plates. Undamaged and damaged steel and aluminum beams are simulated to compare to experimental impedance responses. An aluminum round plate with PZT patch in center is simulated to investigate sensitive range of impedance responses. Finally, numerical analysis of the impedance-based damage monitoring is performed for a steel column connection in which connection bolts are simulated as bolt-loosening. From the numerical simulation test, the applicability of the impedance-based monitoring to the target steel column connection can be evaluated.

2. Impedance-based damage monitoring method

Over the last decade, piezoelectric materials have been widely adopted for SHM applications (Park *et al.* 2003). The advantages of piezoelectric material are cheap, lightweight, robust, and multi-form ranging from thin patches to complex shapes. Piezoelectric materials are commonly used as both sensor (i.e., direct effect) and actuator (i.e., inverse effect) for SHM applications. One of key characteristics is the utilization of the direct effect to sense structural deformation in addition to the inverse piezoelectric effect to actuate the structure (Ho 2012).

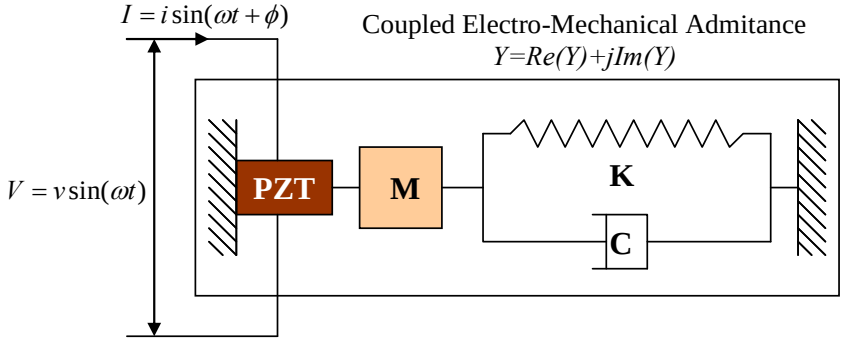

Fig. 1 1-D model E/M interaction between piezoelectric patch and host structure

The E/M impedance response is based on the coupling of mechanical and electrical characteristics (Liang *et al.* 1994). As shown in Fig. 1, the interaction between the PZT patch and the host structure is conceptually explained as an idealized 1-D electro-mechanical relation. The host structure is described as the effects of mass, stiffness, damping, and boundary condition. The PZT patch is modeled as a short circuit powered by a harmonic voltage or current.

When a PZT patch is surface-bonded to a structure, the electrical admittance (the inverse of electro-mechanical impedance $Z(\omega)$) of the patch, $Y(\omega)$ (units Siemens or ohm^{-1}), is a combined function of the mechanical impedance of the host structure, $Z_s(\omega)$, and that of the piezoelectric patch, $Z_a(\omega)$

$$Y(\omega) = j\omega \frac{w_p l_p}{t_p}\left(\left(\overline{e_{33}^{\sigma}} - d_{31}^2 \overline{Y_{11}^E}\right) + \frac{Z_a(\omega)}{Z_a(\omega) + Z_s(\omega)} d_{31}^2 \overline{Y_{11}^E}\left(\frac{\tan kl_p}{kl_p}\right)\right) \tag{1}$$

where $\overline{Y_{11}^E} = (1 + j\eta)Y_{11}^E$ is the complex Young's modulus of the zero-electric field; $\overline{e_{33}^{\sigma}} = (1 - j\delta)e_{33}^{\sigma}$ is the dielectric constant of piezoelectric wafer; d_{31} is the piezoelectric coupling constant in the direction 1 at zero stress; $k = \omega\sqrt{\rho / \overline{Y_{11}^E}}$ is the wave number that depends on mass density ρ and Young's modulus $\overline{Y_{11}^E}$ of the piezoelectric material; and w_p, l_p, and t_p are the width, length, and thickness of the piezoelectric transducer, respectively. The parameters η and δ are the structural damping loss factor and the dielectric loss factor of piezoelectric material, respectively.

In Eq. (1), the first term of the equation is the capacitive admittance of the free piezoelectric patch. The second term includes the mechanical impedance of both the piezoelectric patch and the host structure. The mechanical impedance of the host structure $Z_s(\omega)$ is the ratio of PZT force, f_{PZT}, to structural velocity, $\dot{x}_{PZT}$, at PZT location, as follows

$$Z_s(\omega) = \frac{f_{PZT}}{\dot{x}_{PZT}} = \frac{F_{PZT} e^{i\omega t}}{\dot{x}_{PZT}} \tag{2}$$

If the structure is considered as a system of single degree of freedom, the mechanical

impedance of the host structure can be expressed as

$$Z_s(\omega) = m\omega j + c - \frac{k}{\omega} j \tag{3}$$

Eq. (3) shows that the mechanical impedance of the host structure is a function of mass (m), stiffness (k) and damping (c). Therefore, any changes in dynamic characteristics of the structure could be represented in the change in E/M impedance.

The basic concept of the impedance-based SHM is to monitor the variations in structural mechanical impedance caused by the presence of damage. However, it is not easy to measure the structural mechanical impedance features. As an altering way, impedance methods utilize the electrical impedance of piezoelectric materials. As described in Eq. (1), the electrical impedance of the piezoelectric patch bonded onto a host structure is directly related to the mechanical impedance of the structure. When damage occurs on a structure, its mechanical impedance will be changed. Hence, any changes in the electrical impedance signatures (e.g., frequency shift or magnitude change) are attributed to damage or changes in the structure. In practice, the electric current is measured and used to calculate the E/M impedance as follows

$$Z(\omega) = \frac{V(\omega)}{I(\omega)} = \mathrm{Re}\{Z(\omega)\} + j\,\mathrm{Im}\{Z(\omega)\} \tag{4}$$

where $V(\omega)$ is the input voltage for the PZT sensor; $I(\omega)$ is the electric current; and $\mathrm{Re}\{Z(\omega)\}$, $\mathrm{Im}\{Z(\omega)\}$ are the real part, imaginary part of E/M impedance, respectively.

Bhalla and Soh (2003) demonstrated that the real part is more sensitive to structural damage than the imaginary part. Therefore, the real part is utilized for impedance-based SHM applications. In order to ensure high sensitivity to incipient damage, the electrical impedance must be measured at high frequency range. Since, at high frequencies, the excited wavelength is small and is sensitive enough to detect minor changes in structural integrity. Additionally, high-frequency signals require very low voltage to produce a useful impedance excitation in host structure.

In order to quantify the change in impedance signatures due to structural damage, root mean square deviation (RMSD) of impedance signatures is used. The RMSD is calculated from impedance signatures measured before and after damage as (Sun *et al.* 1995)

$$RMSD(Z, Z^*) = \sqrt{\frac{\sum_{i=1}^{N}\left[Z^*(\omega_i) - Z(\omega_i)\right]^2}{\sum_{i=1}^{N}\left[Z(\omega_i)\right]^2}} \tag{5}$$

where $Z(\omega_i)$ and $Z^*(\omega_i)$ are the impedance signatures measured before and after damage for the i^{th} frequency, respectively; and N denotes the number of frequency points in the sweep. The RMSD is larger than 0 if damage, and vice versa.

Due to experimental and environmental errors, however, the RMSD may be larger than 0 although damage is not occurred. To deal with the uncertain conditions, the control chart analysis is used for decision-making out of the RMSD values. In this study, the upper control limit (UCL) is adopted for alarming damage occurrence, as follows

$$UCL_{RMSD} = \mu_{RMSD} + 3\sigma_{RMSD} \tag{6}$$

where μ_{RMSD} and σ_{RMSD} are mean and standard deviation of RMSDs, respectively. The occurrence of damage is indicated when the RMSD values are larger than the UCL, and vice versa. The impedance-based damage monitoring method using RMSD of impedance signatures is performed as the follows: (1) to measure *n* sets of impedance signals from a PZT sensor for undamaged state; (2) to calculate RMSD of Eq. (5) between impedance signatures of the first data set and the other data sets; (3) to determine the UCL by using Eq. (6); and (4) to continuously monitor RMSD values for damaged states. The occurrence of damage is alerted when the RMSD exceeds the UCL; otherwise, no indication of damage when the RMSD is below the UCL level.

3. Feasibility verification of numerical impedance simulation

In order to demonstrate the applicability of the impedance-based SHM method, numerical simulations are carried out on aluminum and steel structures. COMSOL Multiphysics 4.0 software which is efficient for E/M impedance simulation was employed to estimate models. Steel and aluminum beams and an aluminum round plate were simulated to compare to experiments and to diagnosis occurrence of cracks. A bolted connection in steel column was model to monitor bolt-loosening. In the finite element (FE) models, solid element was used for host structure, and piezoelectric element was used for PZT patch.

3.1 Verification example 1: uncracked steel beams

Four uncracked steel beams which are different from dimensions were simulated to compare to experimental results from Giurgiutiu and Zagrai (2002), as shown in Fig. 2. A thin 7-mm square PZT 5-A patch was boned on each beam. The distance from left end of beam to PZT patch was 40 mm. A voltage 2 V was applied to PZT patch. The beams' properties and PZT patch's properties are summarized in Tables 1 and 2, respectively. In the experiment, impedance signals measured by HP 4194A Impedance Analyzer was performed in the 1 ~ 30 kHz range. The boundary conditions of beams were free. Fig. 3 shows the FE model of the beams.

The comparisons between FE model and experiment are shown in Fig. 4 and listed in Table 3. The resonant frequencies increase proportionally to the thick of beam. The numerical impedance responses are good match with the experimental ones. The differences of resonant frequency are 0.1 ~ 5.1%. Therefore, COMSOL is reliable software for simulation of E/M impedance responses.

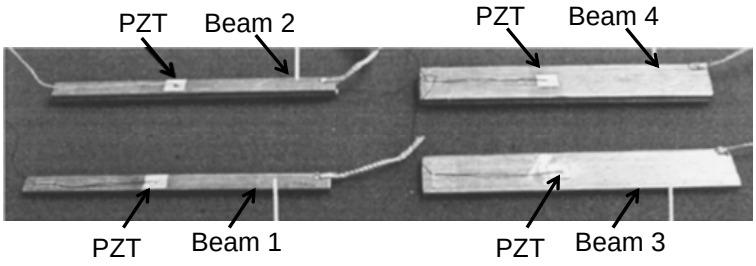

Fig. 2 Steel beams for impedance test (Giurgiutiu and Zagrai 2002)

Table 1 Properties of steel beams

Beam	Dimensions (mm)			E (GPa)	ρ (kg/m^3)	Damping coeff. (%)
	b	l	h			
1	8	100	2.6	200	7750	1
2	8	100	5.2	200	7750	1
3	19.6	100	2.6	200	7750	1
4	19.6	100	5.2	200	7750	1

Table 2 Properties of PZT patch used for steel beams

PZT	Dimensions (mm)			ρ (kg/m^3)	Damping coeff. (%)	Dielectric constant
	b	l	h			
5-A	7	7	0.2	7750	0.5	0.02

Table 3 Comparison of resonant frequencies of steel beams

Peak Freq.	Beam 1			Beam 2			Beam 3			Beam 4		
	Exp. (kHz)	FE (kHz)	Error (%)	Exp. (kHz)	FE (kHz)	Error (%)	Exp. (kHz)	FE (kHz)	Error (%)	Exp. (kHz)	FE (kHz)	Error (%)
1	1.39	1.4	0.7	2.81	2.7	4.0	1.36	1.4	2.7	2.78	2.7	2.8
2	3.80	3.7	2.5	7.45	7.3	2.1	3.76	3.8	1.2	7.44	7.4	0.5
3	7.41	7.3	1.4	13.91	14.1	1.4	7.38	7.4	0.3	13.93	14.3	2.7
4	12.14	12.1	0.3	20.65	-	-	12.09	12.3	1.7	21.83	-	-
5	17.98	18.0	0.1	21.79	22.9	5.1	17.97	18.3	1.9	22.16	23.1	4.2
6	24.84	25.0	0.6	-	-	-	24.85	-	-	-	-	-
7	26.32	25.4	3.5	26.16	25.4	2.9	26.09	25.6	1.9	26.10	25.4	2.7

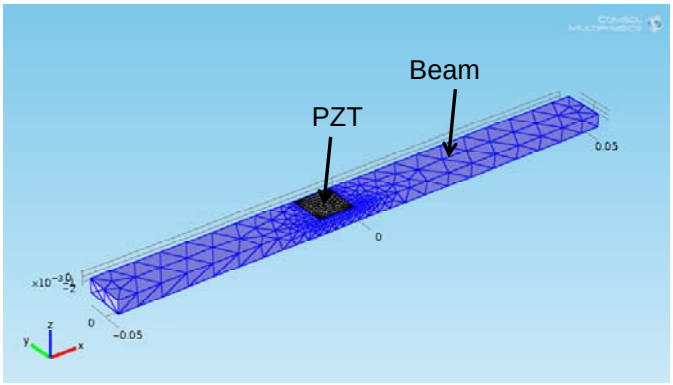

Fig. 3 FE model of steel beams with PZT patch

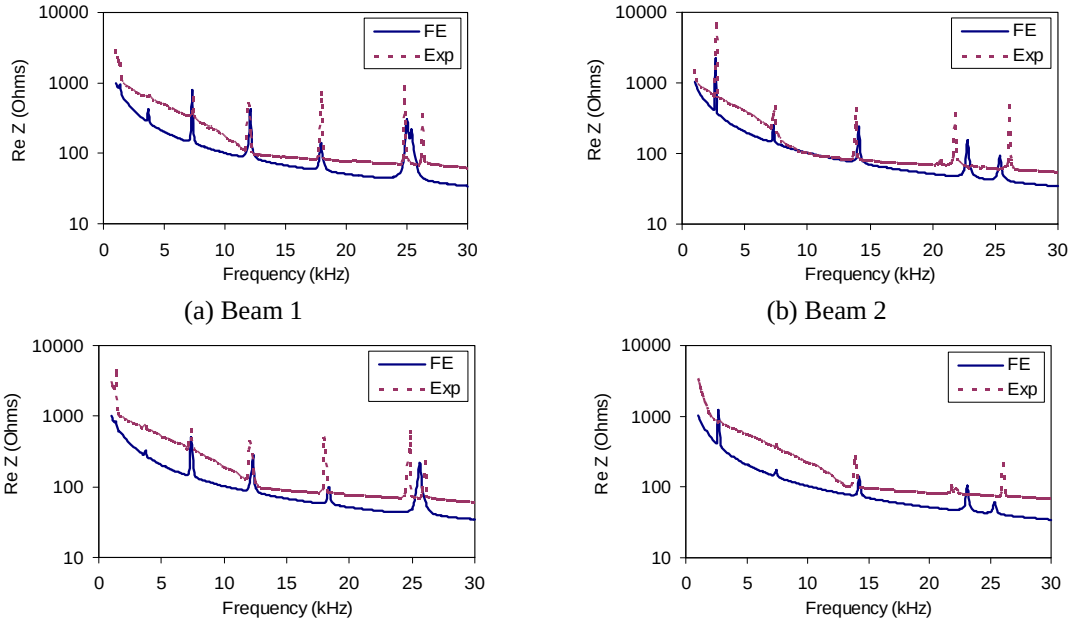

(a) Beam 1 (b) Beam 2

(c) Beam 3 (d) Beam 4

Fig. 4 Real impedance signatures of steel beams: FE simulation versus experiment

3.2 Verification example 2: cracked aluminum beams

In this section, a FE model of aluminum beam was made to detect the occurrence of crack. The beam's dimensions were 1000×20×2 mm; the boundary conditions were free. As shown in Fig. 5, a thin 1000×10×0.5-mm PZT patch was bond on beam at location 62.5 mm from left end. Crack was cut at center with two depths of 3 mm and 6 mm. A voltage 0.5 V was applied to PZT patch. The beam's properties and PZT patch's properties are summarized in Table 4 and Table 5, respectively (Liu and Jiang 2009). Fig. 6 shows the FE model of the beam.

Fig. 7 shows the real impedance responses for uncracked and cracked conditions. As shown in Fig. 7(b), the real impedance signatures shift to the left side when the crack size increases from 0 ~ 6 mm. These results are very similar to ones from Liu and Jiang (2009). A little difference may cause by bonding layer which did not consider in FE model. In order to evaluate this effect, the RMSD of impedance signatures was computed by Eq. (5). From the results shown in Fig. 8, it is observed that the RMSD of impedance tends to increase as the crack size increases. As a result, the occurrence of cracks was successfully detected by using RMSD of impedances.

Fig. 5 Cracked aluminum beam for impedance test (Liu and Jiang 2009)

Table 4 Properties of aluminum beam

Elastic modulus (N/m^2)	E	72.5E9
Mass density (kg/m^3)	ρ	2700
Poisson's ratio	v	0.345

Table 5 Properties of PZT patch used for aluminum beam

Mass density (kg/m^3)	ρ	7750
Elasticity constant (N/m^2)	$C_{11} = C_{22}$	9.74E10
	C_{12}	5.03E10
	$C_{13} = C_{23}$	4.73E10
	C_{33}	7.93E10
	C_{44}	2.3485E10
	$C_{55} = C_{66}$	1.9E10
Electrical permittivity (F/m)	$\varepsilon^T_{11} = \varepsilon^T_{22}$	9.164E-9
	ε^T_{33}	6.906E-9
Piezoelectric stress coeff. (C/m^2)	e_{31}	−8.70279
	e_{33}	17.56576
	e_{15}	14.411

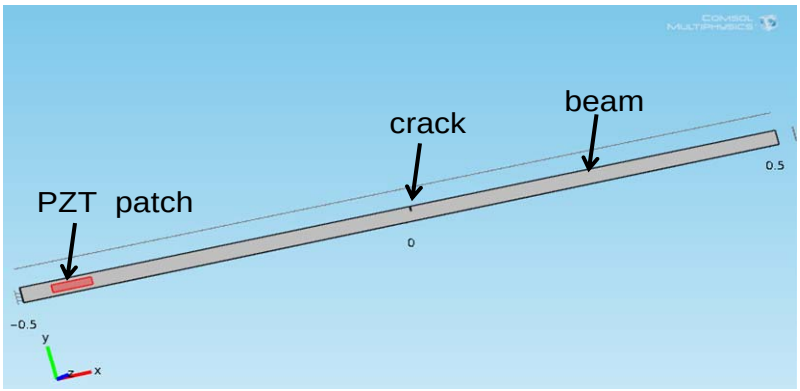

Fig. 6 FE model of cracked aluminum beam

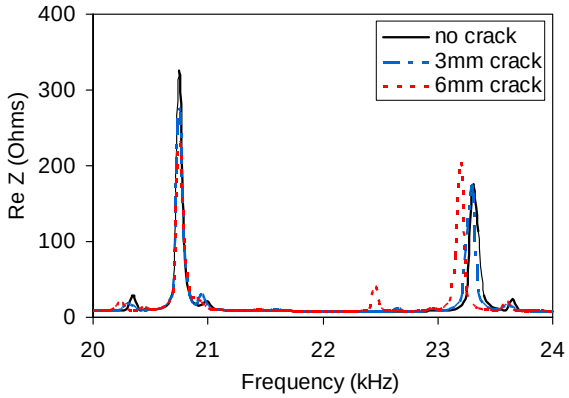

(a) 20 ~ 24 kHz

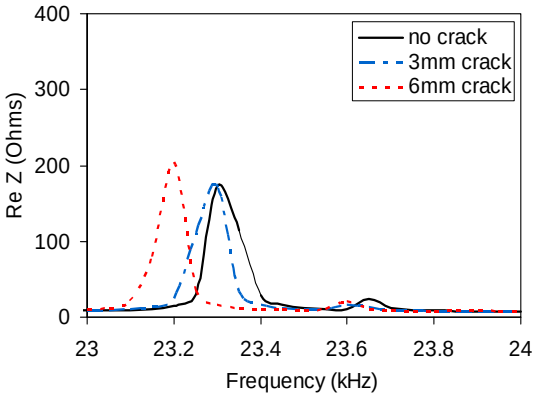

(b) 23 ~ 24 kHz

Fig. 7 Real impedance signatures of aluminum beam

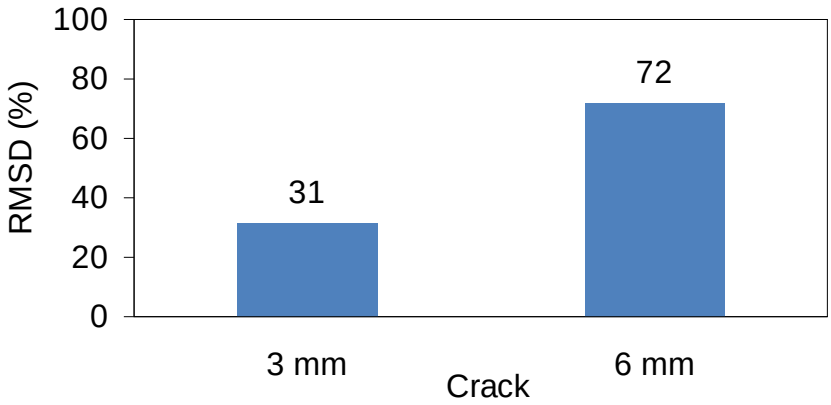

Fig. 8 RMSDs of impedance signatures for two crack sizes

3.3 Verification example 3: round aluminum plate

A round aluminum plate was simulated to diagnosis of cracks and to investigate sensitive range of impedance responses. The FE models of five plates were simulated the same to the experiments from Giurgiutiu and Zagrai (2005). The diameter of each plate was 100 mm and the thickness was 0.8 mm. Each plate was bonded a 7-mm diameter PZT patch at its center. Group 0 was uncracked; groups 1 ~ 4 were cracked with decreasing distance from the PZT patch. A 10-mm circumferential slit was used to simulate the crack. The radial positions 40, 25, 10, and 3 mm from the PZT patch were considered. In the experiment, the plates were placed on foam for free boundary conditions, as shown in Fig. 9. A voltage 1.5 V was applied to each PZT patch. The plates' properties and PZT patch's properties are summarized in Tables 6 and 7, respectively. The impedance signatures were measured by HP 4194A Impedance Analyzer for three frequency ranges: 10 ~ 40 kHz, 10 ~ 150 kHz, and 300 ~ 450 kHz (Giurgiutiu and Zagrai 2005). Figure 10 shows the FE model of the plates.

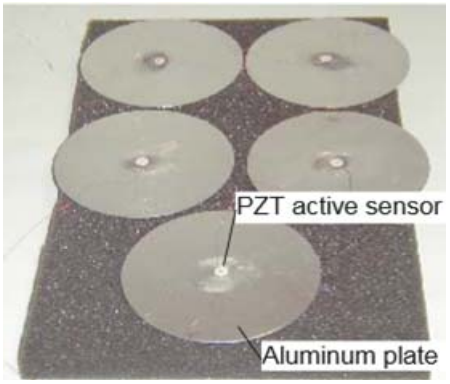

Fig. 9 Round aluminum plate (Giurgiutiu and Zagrai 2005)

As listed in Table 8 and shown in Fig. 11, the numerical and experimental impedances are well agreement. The errors of resonant frequencies are less than 10%. The numerical peak frequencies shift to left side in comparison to experimental ones. Fig. 12 shows the real impedance responses for numerical simulations (Group 0 ~ Group 4). An appropriate frequency range should be selected to get reliable SHM results. In this study, frequency range 300 ~ 450 kHz was selected to computed RMSD of impedance signatures by Eq. (5). As shown in Fig. 13, it is observed that the RMSD of impedance increases as the crack distance decreases. The results are similar to experiments from Giurgiutiu and Zagrai (2005).

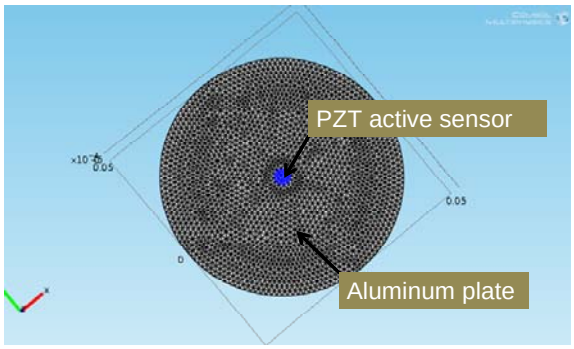

Fig. 10 FE model of round aluminum plate

Table 6 Properties of round aluminum plate

Elastic modulus (N/m^2)	E	70E9
Mass density (kg/m^3)	ρ	2700
Poisson's ratio	v	0.33

Table 7 Properties of PZT patch used for round aluminum plate

Mass density (kg/m^3)	ρ	7750
Elasticity constant (N/m^2)	$C_{11} = C_{13}$	12.0346E10
	C_{12}	75.1791E10
	$C_{14} = C_{15}$	75.1791E10
	C_{16}	11.0867E10
	C_{66}	22.5734E10
	$C_{25} = C_{36}$	21.0526E10
Piezoelectric stress coeff. (C/m^2)	$e_{13} = e_{16}$	−5.35116
	e_{23}	15.7835
	$e_{25} = e_{31}$	12.2947

Table 8 Comparison of resonant frequencies for uncracked plate (Group 0)

Peak	1	2	3	4	5	6	7	8
Exp. (Hz)	799	3168	7182	12844	20053	28844	36348	39115
FE (Hz)	725	3050	6950	12425	19475	28150	35525	38425
Error (%)	9.26	3.72	3.23	3.26	2.88	2.41	2.26	1.76

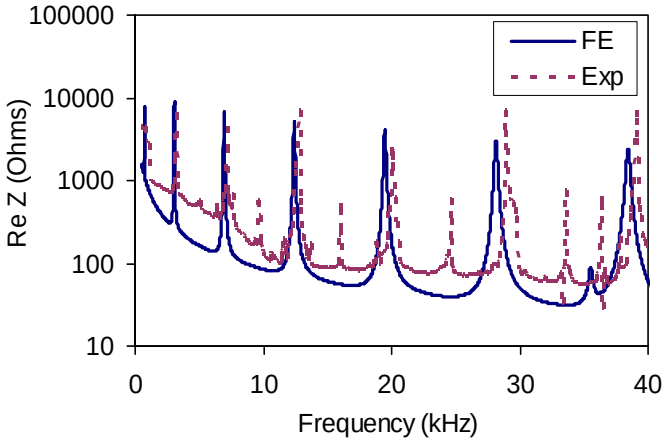

Fig. 11 Real impedance of Group 0 of round plate: FE simulation versus experiment

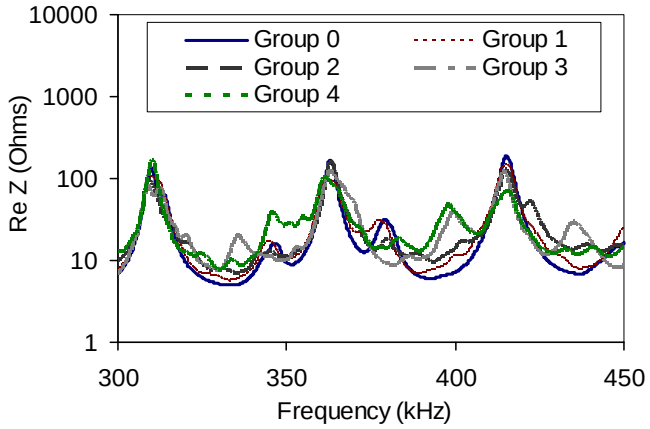

Fig. 12 Simulation of impedance signatures for four groups of round plate

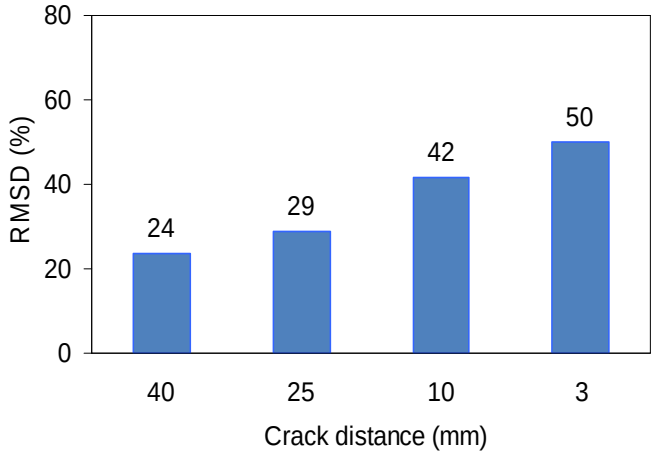

Fig. 13 RMSD values versus crack distance of round plate

4. Impedance monitoring simulation for steel column connection

For steel structures, bolted connections are widely used and bolt-loosening is an important target for SHM. In this study, a bolted connection in steel column was simulated to monitor the bolt-loosening issue. The connection which used to connect two sections H-330×220×8×10 mm included two plates 470×220×10 mm, four stiffeners 220×70×8 mm, four stiffeners 220×100×8 mm, and eight bolts M18. Material properties of steel were defined as modulus of elasticity E = 200 GPa, mass density ρ = 7850 kg/m^3, Poisson's ratio ν = 0.33, and damping coefficient ζ = 0.01. A 20×20×0.2-mm PZT-5A patch was bonded at each bolt. Material properties of PZT patch were defined as modulus of elasticity E = 67 GPa, mass density ρ = 7750 kg/m^3, Poisson's ratio ν = 0.31, and damping coefficient ζ = 0.023. A voltage 5 V was applied to each PZT patch.

Table 9 Bolt-loosening scenarios

Level	Torque (kNm)	Fastener tension force (kN)	Assigned force* (kN/m^2)
0% (Undamage)	172E-3	69	217E3
10%	155E-3	62	196E3
25%	129E-3	52	163E3
50%	86E-3	35	109E3

*Assigned force = Fastener tension force/ Area of washer

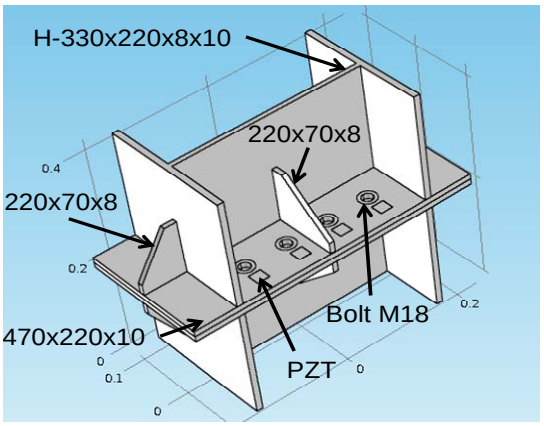

(a) Steel column connection

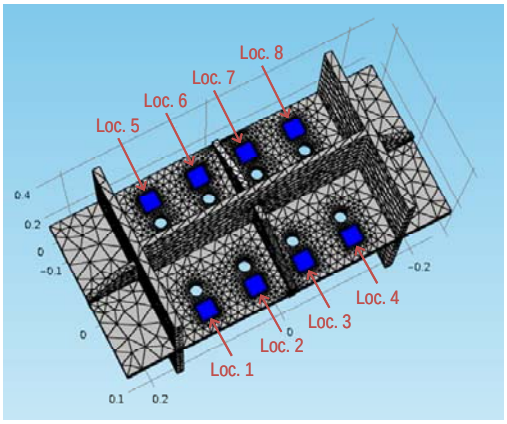

(b) Location of bolts and PZTs

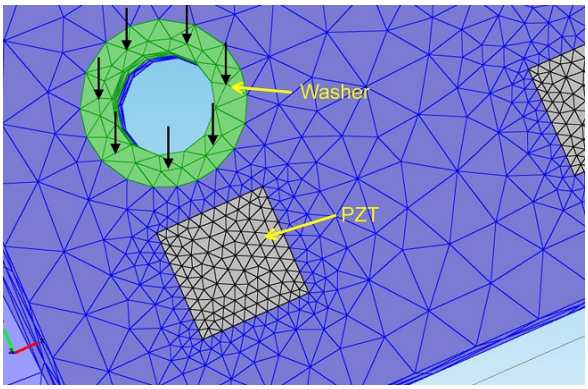

(c) Assigned force

Fig. 14 FE model of steel column connection

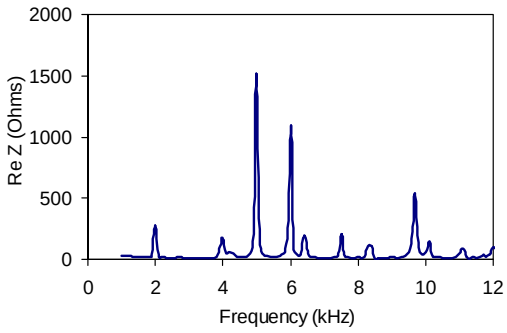

(a) PZT1

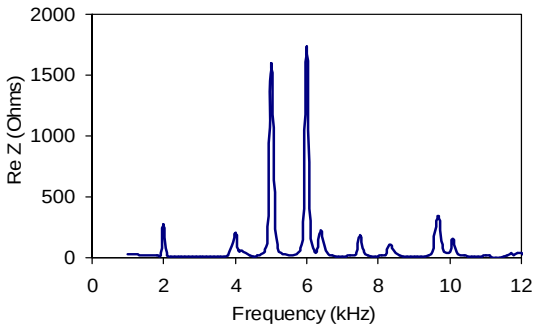

(b) PZT2

Fig. 15 Real impedance signatures of steel column connection

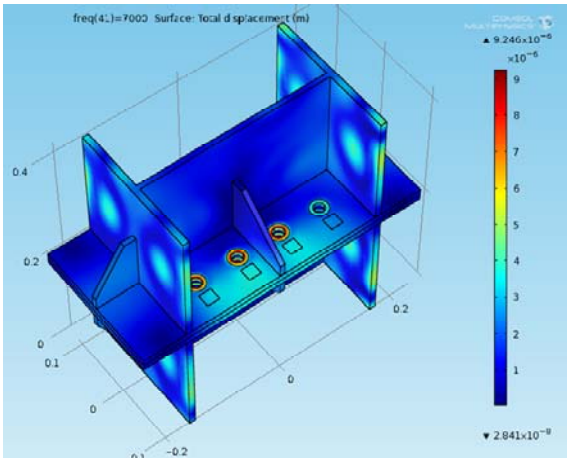

Fig. 16 Deformed shape of steel column connection

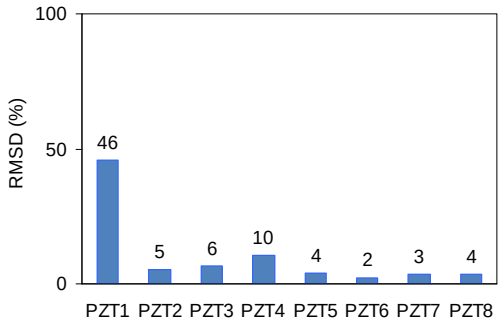

(a) Bolt 1-lossening 10%

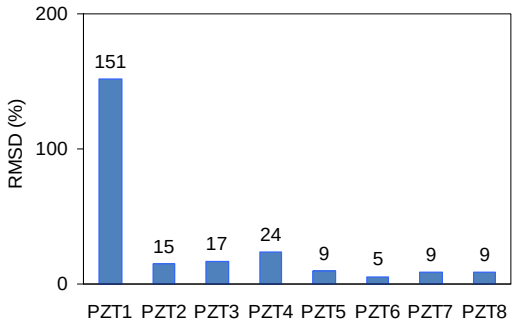

(b) Bolt 1-lossening 25%

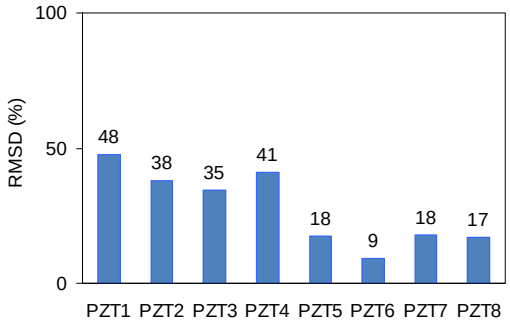

(c) Bolt 1-lossening 50%

Fig. 17 RMSD values versus bolt 1-loosening of steel column connection

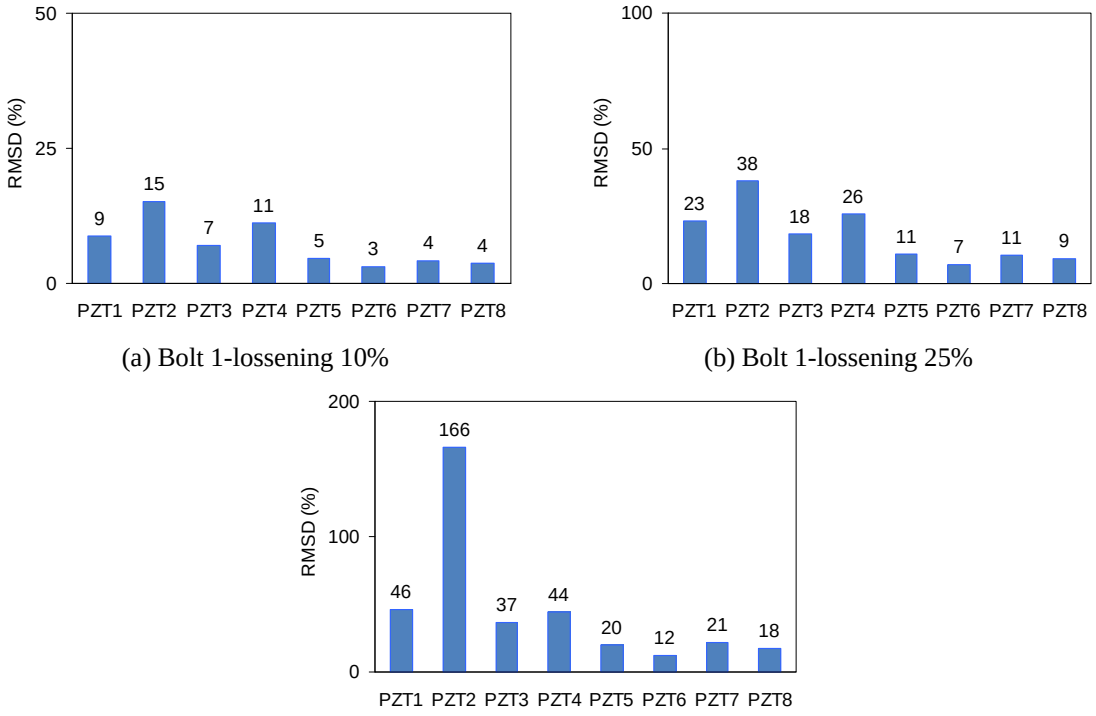

(a) Bolt 1-lossening 10%

(b) Bolt 1-lossening 25%

(c) Bolt 1-lossening 50%

Fig. 18 RMSD values versus bolt 2-loosening of steel column connection

The FE model is shown in Fig. 14. Bolt-loosening of each bolt was simulated at three levels 10%, 25%, and 50%. The bolt-loosening scenarios are listed in Table 9. The fastener tension forces were calculated from the corresponding torque (Nassar *et al*. 2005). In the FE model, the bolt-loosening levels were simulated by reducing the assigned forces on corresponding washers, as shown in Fig. 14(c). The impedance signatures were analyzed in range 1 ~ 12 kHz with increment step of 200 Hz. Fig. 15 shows the real impedance signatures of PZT1 and PZT2. Fig. 16 shows the displacement of structure under applied voltage on PZT patches. The displacement gets high value at the bolts; it proves that the PZT patches are sensitive enough to detect the bolt-loosening. The RMSD of impedance signatures computed by Eq. (5) for frequency range 3 ~ 7 kHz are shown in Figs. 17 and 18.

The RMSD index is highest at the corresponding bolt-loosening. When the level of damage increases, the RMSD increases. Due to the sensitivity of PZT patches bonding near loose bolt, the corresponding RMSD indices are not equal 0; however, these values are much less than the RMSD index at damaged location. Additionally, the stiffness of H-columns and stiffeners also effect to the sensing of PZT patches on connection. In summary, the bolt-loosening issue in the bolted connection in steel column was successfully detected by using impedance responses.

6. Conclusions

In this paper, the practicality of numerical simulation of impedance monitoring for damage detection in steel column connection was evaluated. First, the theory of impedance-based damage monitoring was outlined. Next, the feasibility of numerical simulation of impedance monitoring was verified for several pre-published experimental examples on steel beams, aluminum beams, and aluminum round plates. Finally, numerical analysis of the impedance-based damage monitoring was performed for a steel column connection in which connection bolts were simulated as bolt-loosening.

Numerical verifications were successfully performed for impedance-based damage detection of bolted connection in steel column. From the results, the following conclusions have been drawn as follows:

(1) Numerical simulations of electro-mechanical impedance responses were well estimated. The impedance responses showed good agreement between numerical results and experimental ones. The occurrence of cracks was successfully alarmed by using impedance-based method. The change in impedance responses was more sensitive as the location of crack was closer to PZT sensor.

(2) The bolt-loosening issue was also accurately diagnosed by using impedance-based method. From the numerical simulation test, the applicability of the impedance-based monitoring to the target steel column connection could be well evaluated. It is also observed that the numerical simulation test has potential for the preliminary design of impedance monitoring of real structures in practice.

Acknowledgements

The authors would like to acknowledge the support of Ho Chi Minh City University of Technology's Research Fund. This study was also supported by the Brain Korea 21 (BK21Plus) program of Korean Government.

References

Ayres, J.W., Lalande, F., Chaudhry, Z. and Rogers, C.A. (1998), "Qualitative impedance-based health monitoring of civil infrastructures", *Smart Mater. Struct.*, **7**(5), 599-605.

Bhalla, S. and Soh, C.K. (2003), "Structural impedance based damage diagnosis by piezo-transducers", *Earthq. Eng. Struct. D.*, **32**(12), 1897-1916.

Chaudhry, Z., Lalande, F., Ganino, A. and Rogers, C.A. (1996), *Monitoring the integrity of composite patch structural repair via piezoelectric actuators/sensors*, *AIAA-1996-1074-CP*.

Doebling, S.W., Farrar, C.R. and Prime, M.B. (1998), "A summary review of vibration-based damage identification methods", *Shock Vib. Dig.*, **30**(2), 91-105.

Farrar, C.R. (2001), *Historical overview of structural health monitoring*, Lecture Notes on Structural Health Monitoring Using Statistical Pattern Recognition, Los Alamos Dynamics, Los Alamos, NM.

Giurgiutiu, V. and Zagrai, A. (2005), "Damage detection in thin plates and aerospace structures with the electro-mechanical impedance method", *Struct. Health Monit,*, **4**(2), 0099-20.

Giurgiutiu, V. and Zagrai, A.N. (2002), "Embedded self-sensing piezoelectric active sensors for online structural identification", *J. Vib. Acoust.*, **124**(1), 116-125.

Ho, D.D. (2012), *Multi-scale smart sensing of vibration and impedance for structural health monitoring of cable-stayed bridge*, Ph.D. Dissertation, Pukyong National University, Korea.
Kim, J.T., Huynh, T.C. and Lee, S.Y. (2014), "Wireless structural health monitoring of stay cables under two consecutive typhoons", *Struct.Monit. Maint.*, **1**(1), 47-67.
Kim, J.T., Park, J.H., Hong, D.S. and Park, W.S. (2010), "Hybrid health monitoring of prestressed concrete girder bridges by sequential vibration impedance approaches", *Eng. Struct.*, **32**(1), 115-128.
Li, H.N., Yi, T.H., Ren, L., Li, D.S. and Huo, L.S. (2014), "Reviews on innovations and applications in structural health monitoring for infrastructures", *Structural Monit. Maint.*, **1**(1), 1-45.
Liang, C., Sun, F.P. and Rogers, C.A. (1994), "Coupled electro-mechanical analysis of adaptive material systems-determination of the actuator power consumption and system energy transfer", *J. Intel. Mat. Syst. Str.*, **5**(1), 12-20.
Liu, X. and Jiang, Z. (2009), "Design of a PZT patch for measuring longitudinal mode impedance in the assessment of truss structure damage", *Smart Mater. Struct.*, **18**(12), ID125017.
Min, J., Park, S., Yun, C.B. and Song, B. (2010), "Development of a low-cost multifunctional wireless impedance sensor node", *Smart Struct. Syst.*, **6**(5-6), 689-709.
Nassar, S.A., Barber, G.C. and Zuo, D. (2005), "Bearing friction torque in bolted joints", *Tribilogy Transactions*, **48**, 69-75.
Park, G., Sohn, H., Farrar, C. and Inman, D. (2003), "Overview of piezoelectric impedance-based health monitoring and path forward", *Shock Vib. Dig.*, **35**(6), 451-463.
Park, S., Ahmad, S., Yun, C.B. and Roh, Y. (2006), "Multiple crack detection of concrete structures using impedance-based structural health monitoring techniques", *Exp. Mech.*, **46**(5), 609-618.
Park, S., Yun, C.B., Roh, Y. and Lee, J. (2005), "Health monitoring of steel structures using impedance of thickness modes at PZT patches", *Smart Struct. Syst.*, **1**(4), 339-353.
Pohl, J., Herold, S., Mook, G. and Michel, F. (2001), "Damage detection in smart CFRP composites using impedance spectroscopy", *Smart Mater. Struct.*, **10**(4), 834-842.
Raju, V. (1998), *Implementing impedance-based health monitoring technique*, Master Thesis, Virginia Polytechnic Institute and State University, Blacksburg, VA.
Soh, C., Tseng, K., Bhalla, S. and Gupta, A. (2000), "Performance of smart piezoceramic patches in health monitoring of a RC bridges", *Smart Mater. Struct.*, **9**(4), 533-542.
Sun, F.P., Chaudhry, Z., Liang, C. and Rogers, C.A. (1995), "Truss structure integrity identification using PZT sensor-actuator", *J. Intel. Mat. Syst. Str.*, **6**(1), 134-139.
Zagrai, A.N. and Giurgiutiu, V. (2001), "Electro-mechanical impedance method for crack detection in thin plates", *J. Intel. Mat. Syst. Str.*, **12**(10), 709-718.